Available online at www.sciencedirect.com
ScienceDirect
International Journal of Fatigue 29 (2007) 1634–1646
International Journal of Fatigue
www.elsevier.com/locate/ijfatigue

Variable amplitude fatigue crack growth, experimental results and modeling

R. Hamam [a], S. Pommier [a,*], F. Bumbieler [b]

[a] Laboratory of Mechanics and Technology Cachan, 61, Avenue du Prés. Wilson, 94235 Cachan, France
[b] French Railway Agency (AEF-SNCF), 21, Avenue Salvador Allende, 94407 Vitry sur Seine, France

Received 13 September 2006; received in revised form 31 January 2007; accepted 2 February 2007
Available online 16 February 2007

Abstract

An incremental model was developed so as to predict the growth of fatigue cracks under complex load spectra. It contains a crack propagation law ($da/dt = \alpha|d\rho/dt|$) and a cyclic elastic plastic constitutive law for the cracked structure $d\rho/dt = f(\phi \propto J, \phi_X^c, \phi_{th}^c, \phi_X^m, \phi_{th}^m)$. The crack growth rate da/dt is a rate of creation of cracked area per unit length of crack front. The plastic flow intensity factor rate $d\rho/dt$ is function of the loading level ϕ and of the thresholds for plastic deformation either within the monotonic or within the cyclic plastic zone. Two internal variables are introduced so as to define each threshold, the first one ϕ_X is associated with internal stresses, while the second one, ϕ_{th}, measures the effective threshold for plastic deformation in the crack tip region. The material parameters in the equations are determined using the finite element method. This identification was performed for a 0.48%C carbon steel. Then various fatigue crack growth experiments have been performed in order to validate the model, monotonic fatigue crack growth experiments at different stress ratios from $R = -1$ to $R = 0.4$, single overloads with overloads factor between 1.5 and 1.8, and bloc loads with X overloads every Y cycles, X and Y varying from one experiment to another. The predictions of the model reproduce well experimental results. Finally the model was applied to an industrial problem: the growth of a semi elliptical crack at the surface of a train wheel. For this purpose, load spectra were measured in situ on a train wheel, it came out that the model had to be extended to biaxial tension-compression and bending loading conditions, which was done.
© 2007 Elsevier Ltd. All rights reserved.

Keywords: Variable amplitude fatigue; Overloads; Stress ratio; Spectrum

1. Introduction

Predicting fatigue crack growth in metals under random loadings is a difficult task, in particular because of load history effects, which are known for decades to stem from plastic deformation in the vicinity of the crack tip [1–6]. In addition, history effects are closely related to the elastic–plastic behaviour of the material [6–9]. Let consider for instance the effect of a single overload. The material ahead of the crack tip yields during the application of the overload. As long as the plastic zone of the overload is fully constrained inside the elastic bulk, compressive residual stresses appear at unloading as a consequence of plastic deformation and limit the efficiency of subsequent fatigue cycles. This is at the origin of the well-known overload retardation effect. Besides, the Bauschinger effect of a material makes reverse plasticity within the overload plastic zone easier. In such a case, the overload retardation effect is less marked and somehow delayed [9]. Hence the need to estimate internal stresses in the crack tip region as precisely as possible for each material. For this purpose, a local approach (FEM) is required so as to capture the very details of the elastic–plastic cyclic deformation of the material in the crack tip region. But, in practice, it is common to encounter fatigue lives that reach tens of millions of ''cycles''. Global approaches are then usually preferred to

* Corresponding author. Tel.: +33 1 47 40 28 69; fax: +33 1 47 40 22 40.
E-mail address: pommier@lmt.ens-cachan.fr (S. Pommier).

0142-1123/$ - see front matter © 2007 Elsevier Ltd. All rights reserved.
doi:10.1016/j.ijfatigue.2007.02.005

local (and time consuming) ones. A method was therefore proposed so as to capitalize the advantages of both local and global approaches, i.e. the quality and the precision of the computation on the one hand and the reduced number of degrees of freedom on the other hand [12].

The idea of that method is as follows. The mode I displacement field in the local coordinate system attached to the crack front is assumed to be depicted by its partition into an elastic field and a plastic field. Then, each part of the displacement field is also assumed to be the product of a known reference field, function of space coordinates only, and of an intensity factor, function of the loading conditions. This approximation is only valid in the near crack tip region. The main advantage of this approach is that it reduces drastically the number of degrees of freedom in the problem. As a matter of fact, since the reference fields are assumed to be known, the remaining degrees of freedom are the position of the crack tip and the intensity factors of the elastic and plastic parts of the displacement field, which are correspondingly labelled the effective stress intensity factor $\widetilde{K}_I$ and the plastic flow intensity factor ρ.

To summarize briefly the procedure, the displacement field is computed using the finite element method and a suitable constitutive law for the material. Then the two intensity factors are extracted using the least square method. The results are analysed, at the global scale, by plotting the effective stress intensity factor versus the plastic flow intensity factor. Using this type of results, just as one would use a "stress versus plastic strain" curve, it was possible to build up an empirical model for the cyclic elastic–plastic behaviour of the crack tip region at the global scale [12]. In this model, internal variables had to be defined, which measure the level of internal stresses and the effective thresholds for plasticity in the crack tip region either within the cyclic plastic zone or within the monotonic plastic zone [12–14]. Empirical equations are proposed for their evolutions with respect to the intensity factor of the plastic part of the displacement field and with respect to crack growth.

Using the finite element method and the approximation discussed above, a cyclic elastic–plastic constitutive model was build for the crack tip region at the global scale. This model provides the plastic flow intensity factor rate as a function of the loading level and of the current values of the internal variables [12].

Besides, with the rough assumption that the crack grows because of crack tip plasticity, a linear relation is assumed between the crack growth rate and the plastic flow intensity factor. If necessary, this equation can be modified to account for the effect of the environment, but this is not the object of the present paper.

In this paper, it is discussed how the model can be applied to an industrial problem: the growth of a semi-elliptical crack at the surface of a train wheel. For this purpose, load spectra were measured in situ on a train wheel. The model was identified for the material constituting the train wheel and the predictions of the model are compared to fatigue crack growth experiments under variable amplitude loadings conditions. It came out that the model should be extended to biaxial tension-compression and bending loading conditions. These evolutions are discussed in the following.

2. Position of the industrial problem

Three aspects are indispensable to master railway systems: design, manufacture and maintenance. Maintenance defines surveillance intervals which are defined at present from field experience. The aim of the French Railway Agency (AEF-SNCF) is to use fracture mechanic in order to satisfy to European interoperability imperative of railway stock. The initiation of cracks at the surface of a wheel is usually attributed to foreign object damage (ballast impact). In such a case, cracks are semi elliptic and their growing path is normal to the radial direction of the wheel. The aim of this research is to define the inspection intervals of wheels, i.e. the number of kilometers necessary for a crack to grow from the smallest dimension detectable by non destructive technique (NDT) and the critical crack length. The diameter and the thickness of a wheel are in the order of one meter and 30 mm; whereas the initial crack length is in the order of 1 mm. A crack initiated at the surface of a wheel can therefore be considered as a semi-elliptical crack growing at the surface of a semi-infinite media, with a finite thickness.

So as to characterize the local loading conditions of the train wheel, in situ measurements have been performed by the French Railway Agency. First of all, a 3D finite element model of the wheel was built so as to identify the critical areas of the wheel under various loading conditions (running of the train along a straight line, along a curve...) (Fig. 1b). Then, strain gauges were glued symmetrically onto the internal and external faces of the wheel. Different radius and different angular positions were instrumented, among which the spots identified as the most critical ones.

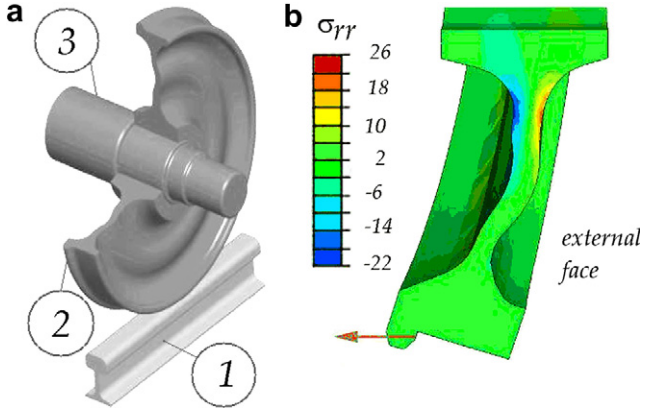

Fig. 1. (a) Schematic of the mounting of a train wheel, (1) the rail, (2) the wheel and (3) the axle. (b) Finite element model of the wheel. Load case: running of the train along a curve.

The strain gauges signals were recorded as a function of time.

These measurements allowed extracting the radial, hoop and shear components of the stress tensor along each side of the wheel during the train running. A short extract of the evolution of the radial stress on each side of the wheel is plotted in Fig. 2a. The train was running along a straight line at 120 km/h which is the least severe situation. In such a case, the external face is mostly in tension while the internal face is under compression in the critical area of the wheel. The finite element analysis of the wheel showed that the stress field across the wheel's thickness is not far from being linear in the area of concern. Therefore, it is possible to extract the bending and the tension-compression components of the stress field across the wheel's thickness (Fig. 2b and c) in the critical area using in situ measurements. The tension-compression part of the stress field is close to constant amplitude loading with a stress ratio equal to -1 (Fig. 2b). But the bending part of the signal is highly variable, even when the train is simply running along a straight line (Fig. 2c).

The same analysis can be performed with the other components of the stress tensor. It is found that the shear component is usually small compared to the radial and hoop ones (Fig. 3a). And finally, the loading is observed to be almost proportional. The bending part of the hoop stress

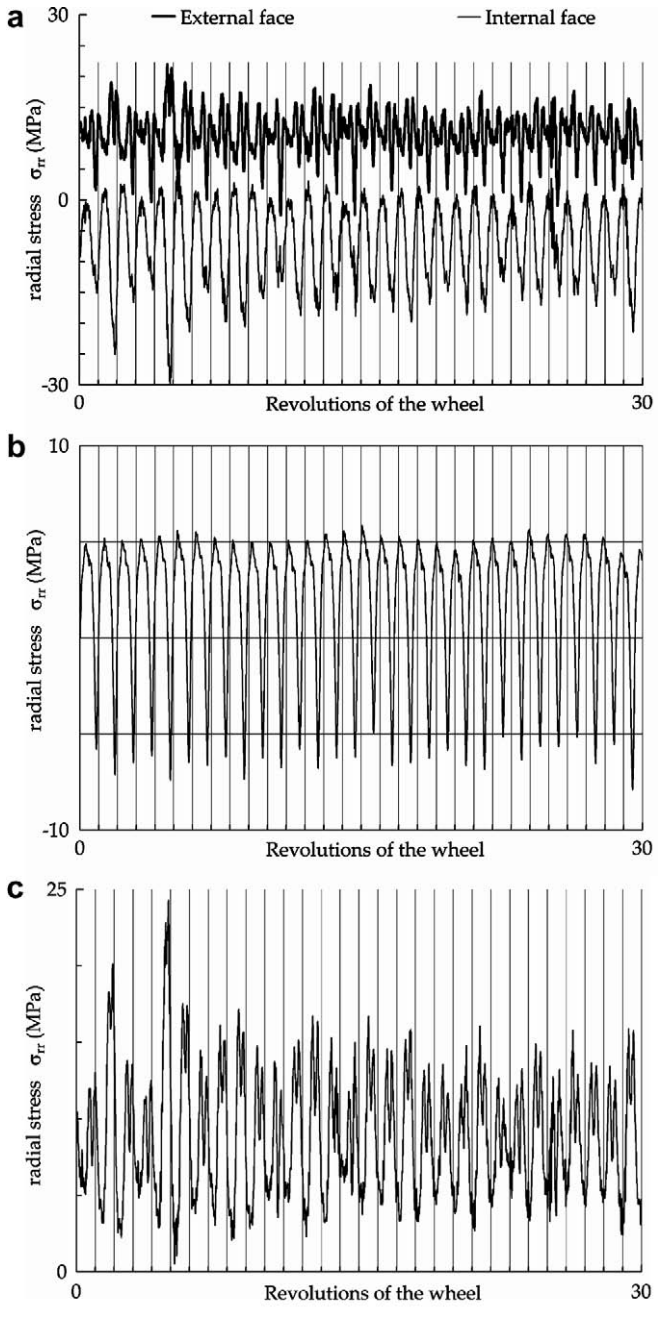

Fig. 2. Evolution of the radial component of the stress tensor during a few revolutions of the wheel. Case of a train running along a straight line. (a) Evolution of the radial stress as measured using strain gauges glued symmetrically onto the internal and the external faces of the wheel. (b) tension-compression part $\sigma_{rr} = (\sigma_{rr}^{ext} + \sigma_{rr}^{int})/2$ and (c) bending part $\sigma_{rr} = (\sigma_{rr}^{ext} - \sigma_{rr}^{int})/2$ of the radial stress along the thickness of the wheel.

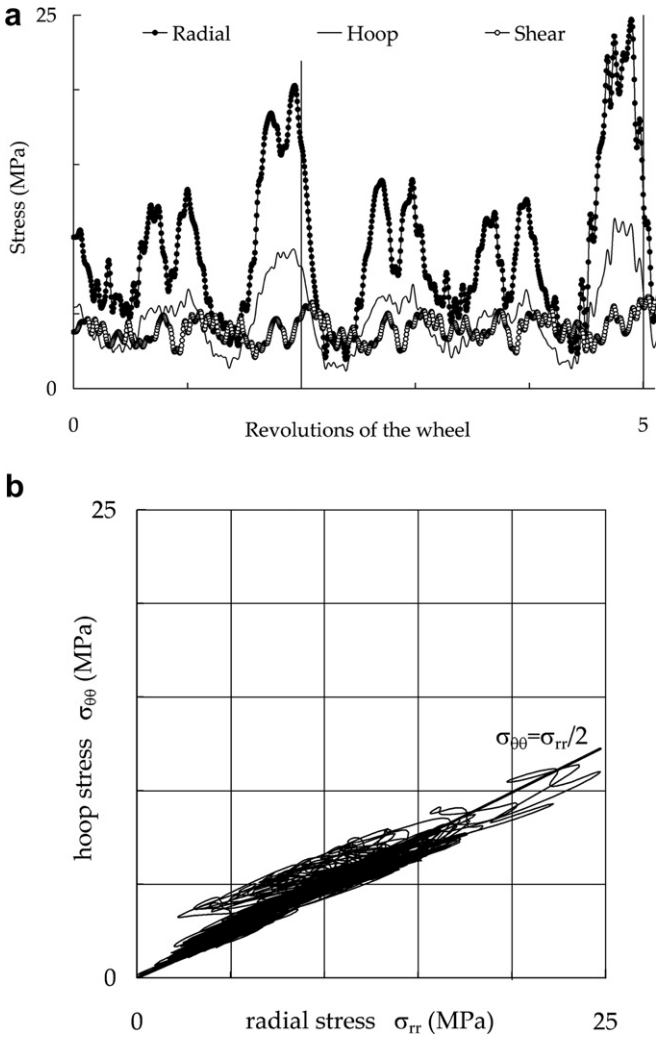

Fig. 3. Bending part $\sigma_i = (\sigma_i^{ext} - \sigma_i^{int})/2$ of the measured stress components. (a) Comparison of the radial, shear and hoop stresses. The shear stress is negligible. (b) Hoop stress versus radial stress, the loading is more or less proportional.

is around one half of the bending part of the radial stress (Fig. 3b).

Finally, the problem can be sketched out as follows. The crack's geometry can be approached by that of a semi-elliptical crack in a semi-infinite plate subjected to biaxial bending and tension-compression loadings [15,16]. The two bending components are proportional. During the running of a train, the bending part of the loading is highly variable. The variable nature of the loading arises from running conditions which vary among straight line, curve or split switch. For a given running condition (straight line for instance) the correlation length in the stress versus time signal is well over a thousands wheel's revolutions. Finally, a train endures around two millions wheel's revolutions per day.

The aim of this study is thus to simulate efficiently the growth of a semi-elliptical crack under variable biaxial tension-compression and bending. For this purpose the parameters of the incremental fatigue crack growth model proposed by Pommier et al. [7,12] were identified for the material of the wheel. Then, the model was validated using the results of various variable amplitude fatigue crack growth experiments. But the model had to be enriched so as to account for the high compression levels that are reached in a wheel disk and for the biaxial loading condition that arise from the axisymmetric geometry of the wheel.

3. Model

3.1. Background

The mode I displacement field in the near crack tip region is assumed to be depicted by its partition into an elastic field and a plastic field. Then, each part of the displacement field is also assumed to be the product of a reference field, function of space coordinates only, and of an intensity factor, function of the boundary conditions (loading, crack geometry...). The main advantage of this approach is that it reduces drastically the number of degrees of freedom in the problem. As a matter of facts, the reference fields are given in the coordinate system attached to the crack front. Therefore, the degrees of freedom in the problem are reduced to: the location of the crack tip and the values of the two intensity factors (Eq. (1)), which are correspondingly labelled, the effective stress intensity factor $\widetilde{K}_{\mathrm{I}}$ and the plastic flow intensity factor ρ:

$$\underline{u}^{\mathrm{FE}}(\underline{x},t) \approx \widetilde{K}_{\mathrm{I}}(t)\underline{u}_{\mathrm{e}}(\underline{x}) + \rho(t)\underline{u}_{\mathrm{p}}(\underline{x}) \tag{1}$$

where $\underline{u}^{\mathrm{FE}}(\underline{x},t)$ is the displacement field as calculated using the FE method and associated with a very small variation around the current configuration of the crack, where $\underline{u}_{\mathrm{e}}(\underline{x})$ is the reference elastic displacement field and $\underline{u}_{\mathrm{p}}(\underline{x})$ the reference plastic field. For each time increment in the computation, the projection proposed in Eq. (1) is performed using a post treatment routine.

From a practical point of view, it is not necessary to have at ones disposal an analytical expression for the fields u_{e} $(\underline{x})$ and $\underline{u}_{\mathrm{p}}(\underline{x})$. The reference elastic field $\underline{u}_{\mathrm{e}}(\underline{x})$ is the numerical solution of a previous finite element computation using the same FE mesh, an elastic behaviour for the material and boundary conditions such as that the nominal stress intensity factor is equal to unity. Similarly a numerical reference solution can be constructed for the plastic field $\underline{u}_{\mathrm{p}}(\underline{x})$ using a mathematical transform that performs a partition such as that proposed in Eq. (1) (i.e. the Karhunen–Loeve transform). However, analytical solutions are useful for interpreting the results. At present the best approximation was obtained with the displacement field around a climb dislocation [10] (Eqs. (2) and (3)):

$$u_{\mathrm{p}}(r,\theta)_x = \frac{1}{\pi(\kappa+1)}[(\kappa-1)\log r - 2\cos^2\theta] \tag{2}$$

$$u_{\mathrm{p}}(r,\theta)_y = \frac{1}{\pi(\kappa+1)}[(\kappa+1)\theta - 2\cos\theta\sin\theta] \tag{3}$$

This solution corresponds to the insertion of a semi-infinite slit of material of thickness 1 in the half plane $y=0$, $x<0$ and it is worth to underline that $:u_{\mathrm{p}}(r,\theta=\pi)_y = 1$. Therefore, ρ measures the plastic part of the displacement in the K-dominance area and can be also interpreted as the plastic part of the CTOD. Besides, $\widetilde{K}_{\mathrm{I}}$ measures the elastic part of the displacement in the K-dominance area.

Provided that the displacement approximated by Eq. (1) is taken as the displacement between consecutive time increments (eulerian approach), the error associated with this approximation remains typically below 10% [12].

This method enables us to generate the evolutions of ρ versus $\widetilde{K}_{\mathrm{I}}$ (Fig. 4). The value of the stress intensity factor $\widetilde{K}_{\mathrm{I}}$ calculated using this method differs slightly from the nominal stress intensity factor K_{I}^{∞}. The difference $K_{\mathrm{I}}^{\mathrm{sh}} = \widetilde{K}_{\mathrm{I}} - K_{\mathrm{I}}^{\infty}$ stems from the shielding effect of internal stresses

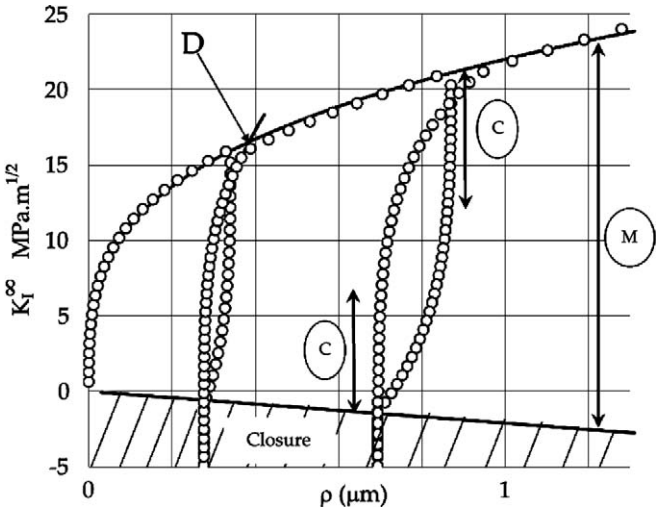

Fig. 4. Evolution of the calculated value of the plastic flow intensity factor ρ versus the nominal stress intensity factor K_{I}^{∞}.

at crack tip [11,12]. This difference is also found to vary linearly with ρ. Therefore, only the evolution of ρ needs to be modelled.

In Fig. 4, the evolution of ρ is plotted against K_I^∞ during a cyclically increasing load sequence. After each load's reversal, there is a domain within which ρ is not varying. Within this domain, the behaviour of the cracked structure can be considered as elastic. The "elastic domain" of the cracked structure ((C) in Fig. 4) varies both in dimension and position. Therefore, two internal variables are introduced to define the yield point of the crack tip region, which are the position and the dimension of its elastic domain. The equivalent in the continuum theory of plasticity would be kinematics and isotropic hardenings of the material. The displacement of the elastic domain is a consequence of the development of internal stresses, the size of the elastic domain is an effective threshold for crack tip plasticity.

Besides, a discontinuity in the evolution of K_I^∞ versus ρ is observed at point D in Fig. 4, when the loading level exceeds the maximum load level reached previously, or in other words, when it reaches the threshold above which the monotonic plastic zone extends again. Therefore an elastic domain is also defined for the monotonic plastic zone, by its size ((M) in Fig. 4) and its position. Since, in mode I, crack closure occurs, the closure point was taken as the definition of the "position" of the elastic domain for the monotonic plastic zone. The displacement of this point is related to the growth of internal stresses at the scale of the monotonic plastic zone.

To these evolutions is associated a model for the elastic–plastic behaviour of the crack tip region at the global scale [12] which was build within the framework of dissipative processes. Firstly it was discussed that the driving force associated with ρ, denoted by ϕ, is proportional to J the Rice's integral. Internal variables have to be defined, that measure the level of internal stresses (ϕ_X^c, ϕ_X^m) and the effective thresholds $(\phi_{th}^c, \phi_{th}^m)$ for plasticity within the cyclic and the monotonic plastic zones [12–14]. Empirical equations are proposed for their evolutions with respect to the variations of the plastic flow intensity factor $\partial\rho$ and to crack growth ∂a.

To summarize briefly, using the finite element method and the approximation in Eq. (1), a cyclic elastic–plastic constitutive model was build for the crack tip region at the global scale. This model provides the plastic flow intensity factor rate as a function of the loading level and of the current values of the internal variables $d\rho/dt = f(\phi \propto J, \phi_X^c, \phi_{th}^c, \phi_X^m, \phi_{th}^m)$ [12].

Besides, it is assumed that there is a linear relation between the crack growth rate and crack tip plasticity: $da/dt = \alpha|d\rho/dt|$, where α is a constant. It is worth to mention that the crack growth rate da/dt, corresponds to the rate of creation of cracked area per unit length of the crack front.

The equations of the model are not provided here, but can be found in other publications [12].

3.2. Identification for a 0.48%C mild steel

So as to identify the parameters of the model using the method described in Section 3.1, it is required to identify the constitutive behaviour of the material of the wheels. For this purpose, push–pull specimens were machined from a high-speed train forged wheel, along the radial and along circumferential directions. The material anisotropy is found to be negligible. The material displays a Lüders peak and a plateau in monotonic tension, but the peak disappears or is significantly reduced in cyclic tests. Therefore, the peak was not taken into account in the constitutive behaviour of the material.

Finally, the constitutive model of the material includes three non-linear kinematics hardening terms and one non-linear isotropic hardening term (Fig. 5 and Table 1). Each non-linear kinematics hardening term obeys the Armstrong–Frederick hardening rule (Eq. (4)):

$$\dot{X}_i = \frac{2}{3} C_i \dot{\varepsilon}_p - \gamma_i X_i \dot{p} \tag{4}$$

And the isotropic hardening is as follows (Eq. (5)):

$$\dot{R} = b(R_0 + Q - R)\dot{p} \quad \text{with} \quad R|_{p+0} = R_0 \tag{5}$$

With:

$$\dot{p} = \sqrt{\frac{2}{3}\underline{\underline{\dot{\varepsilon}}}_p : \underline{\underline{\dot{\varepsilon}}}_p} \tag{6}$$

A very good agreement is obtained between the experimental and the simulated stress–strain curves (Fig. 5).

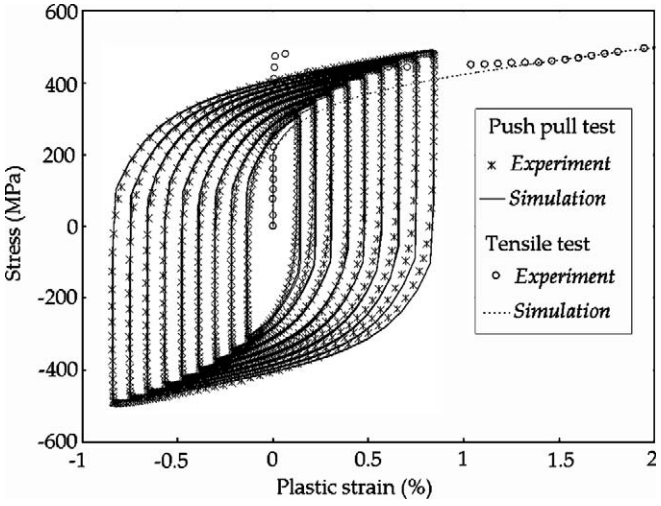

Fig. 5. cyclic-stress strain curves as measured on a 0.48%C steel, comparison between the experiments and the simulation.

Table 1
Material parameters

E	ν	R_0	Q	b	C_1	γ_1	C_2	γ_2	C_3	γ_3
190,000	0.3	210	80	0.53	50,000	1000	32,500	500	11,397	29

Then various finite element analyses were performed so as to identify the cyclic plastic behaviour of the cracked structure from the knowledge of the cyclic plastic behaviour of the material. A refined finite element model was build for the cracked structure and loading–unloading sequences were simulated. The partition proposed in Eq. (1) was performed at each increment of the computation. And the evolution of ρ versus K_I^∞ is determined for the 0.48%C steel employed for the wheels.

An example of such a computation is given in Fig. 6. During an unloading sequence from a point (ρ_0, K_0), ρ is found to remain constant if $K_0 - K(t)$ is below a threshold b_c, then the evolution is found to be roughly proportional to the square root of $\rho_0 - \rho$. The same evolution was found whatever the value of the initial point (ρ_0, K_0) either for a loading or an unloading sequence. This enables us to identify two parameters a_c and b_c employed in the evolution equation $\partial\phi_X^c/\partial\rho$ of the position ϕ_X^c of the elastic domain of the cyclic plastic zone with respect to the variations of ρ, where $\phi_i = ((1-\nu^2)/2E)K_i^2$.

It is useful to underline that if such a relation between ρ and K_I is chosen, with the assumption that the crack growth rate is proportional to the plastic flow intensity factor rate (Eq. (7)), and without taking into account any effects related to the monotonic plastic zone (ϕ_X^m, ϕ_{th}^m), the crack growth rate obeys a relation which is a classical alternative to the Paris' law (Eq. (8)) [17], where b_c is playing the role of an effective threshold for fatigue crack growth:

$$\frac{da}{dt} = \alpha\left|\frac{d\rho}{dt}\right| \tag{7}$$

$$\Delta K = a_c\Delta\rho + b_c \;\&\; \text{Eq. (7)} \Rightarrow \frac{da}{dN} = \frac{2\alpha}{a_c^2}(\Delta K - b_c)^2 \propto (\Delta K - \Delta K_{th}^{eff})^2 \tag{8}$$

An automated protocol was set up so as to identify the entire set of parameters in the model from finite element computations. The set of parameters identified for the 0.48%C mild carbon steel and the set of equations in the model are provided in Appendix 1. At this stage, the constitutive model $d\rho/dt = f(\phi \propto J, \phi_X^c, \phi_{th}^c, \phi_X^m, \phi_{th}^m)$ of plasticity in the crack tip region is fully identified.

Then, a constant amplitude fatigue crack growth experiment is necessary to identify the tuning parameter α in Eq. (7). For this purpose, the experiment was simulated using the model and the results are plotted in a Paris diagram. First, it is observed that the calculated fatigue crack growth rate obeys the Paris law. Besides, the tuning parameter α modifies primarily the coefficient of the Paris law and not its exponent. This exponent is close to 3. The coefficient α is then adjusted so as to obtain the best agreement between the simulation and the experiment (see Fig. 7).

3.3. Validation

The model is identified using push–pull tests (and FE computations) and constant amplitude fatigue crack growth tests. Then, once the model is identified, it also needs to be validated. For this purpose, variable amplitude fatigue crack growth experiments were conducted and compared with the simulations. CCT sample were used, with a thickness of 5 mm. The positions of the two tips of the crack, on each side of the sample were determined optically. The measurement of the total crack length, $2a$, was performed every 1 mm.

The following experiments were performed. First of all (Fig. 8a) the crack was grown up to a length of $2a = 23$ mm under a stress ratio $R = 0$ and a maximum stress level $\Sigma_{max} = 100$ MPa. Then an overload either at $\Sigma_{peak} = 150$ or 180 MPa was applied. And the crack was grown again at $R = 0$ and $\Sigma_{max} = 100$ MPa. A very typical delayed retardation effect is observed in both cases. A reasonable

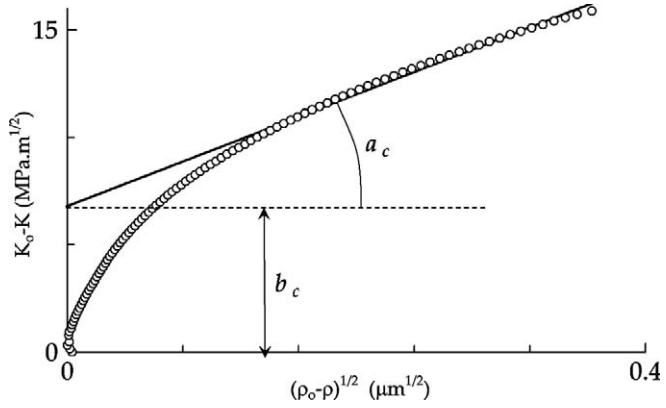

Fig. 6. Simulation of the very beginning of the unloading of the cracked structure from a maximum applied stress intensity factor $K_0 = 21$ MPa m$^{1/2}$ and an initial plastic flow intensity factor equal to $\rho_0 = 1$ μm.

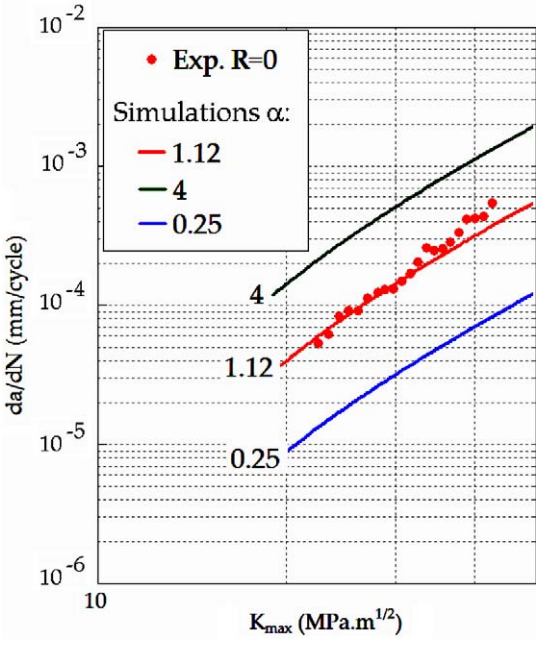

Fig. 7. Comparison between simulations and a constant amplitude fatigue crack growth experiment at $R = 0$ in the 0.48%C mild carbon steel employed for the wheel's. Adjustment of the tuning parameter α in Eq. (7).

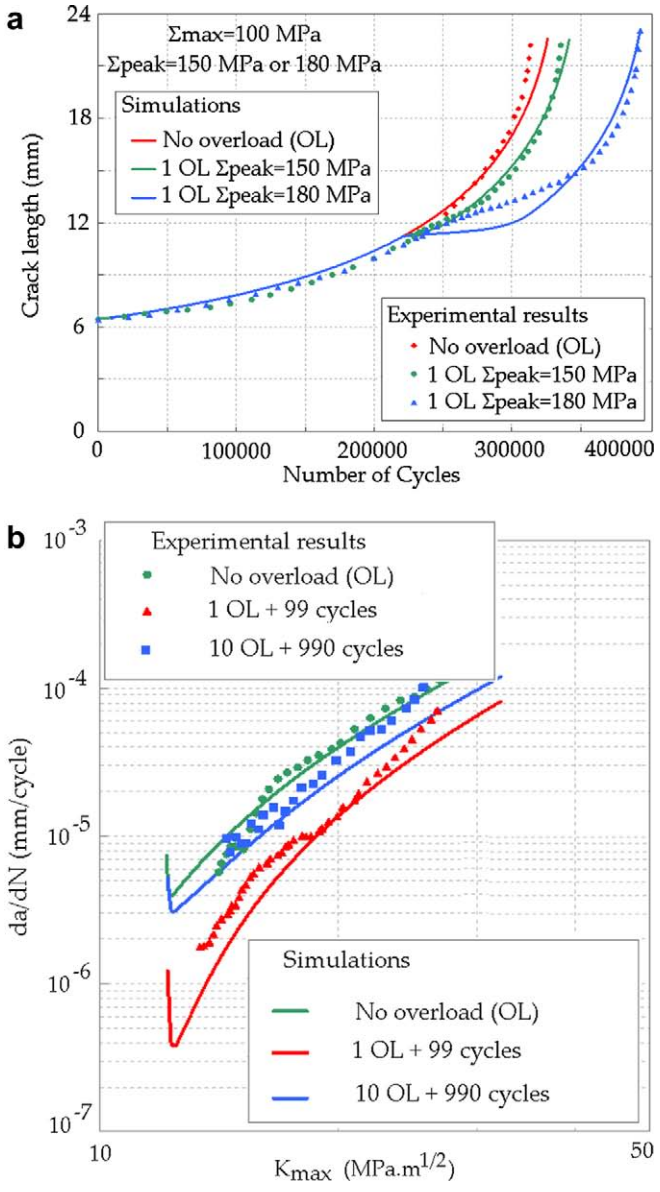

Fig. 8. (a) retardation effect after a single overload. (b) Mean retardation effect of 1% of overloads at $\Sigma_{peak} = 1.5\ \Sigma_{max}$ within a block of either 100 or 1000 cycles.

agreement is found between the simulations and the experiments.

Secondly, (Fig. 8b) the crack was grown under blocks of cycles with 1% of consecutive overloads at $\Sigma_{peak} = 1.5\ \Sigma_{max}$ either in blocks of 100 or in blocks of 1000 cycles. The mean retardation effect is maximum when the block length is of thousand overloads. A good agreement is found between the simulations and the experiments. An experiment was also conducted with 1% of overloads per block of ten thousand cycles. This experiment is not shown here. The mean crack growth rate in that experiment superimposes with that obtained for 1% of overloads per block of 1000 cycles, and the simulations coincide with the experiments.

Thirdly, the simulation of such experiments requires less than 2 min. This demonstrate that the model is applicable in an industrial context.

4. Effect of a compression phase below the closure point

The incremental model was identified and validated using a set of variable amplitude fatigue crack growth experiments. However, the model had to be adapted for the problem of the train's wheel. As a matter of fact, the stress ratio is often below −1. It was therefore necessary to examine the effect of the compression phase below the contact point between the crack faces.

4.1. Finite elements analyses and modelling

The finite element method was employed so as to analyse the effect of a compression phase on the plastic flow intensity factor. For this purpose various simulations have been performed. For instance, the crack was opened, unloaded down to the closure point and reloaded immediately, or reloaded after a significant compression phase below that closure point. The differences in the (ρ, K_I) curves after the re-opening of the crack enables to discuss the effect of the compression phase on the internal variables of the model.

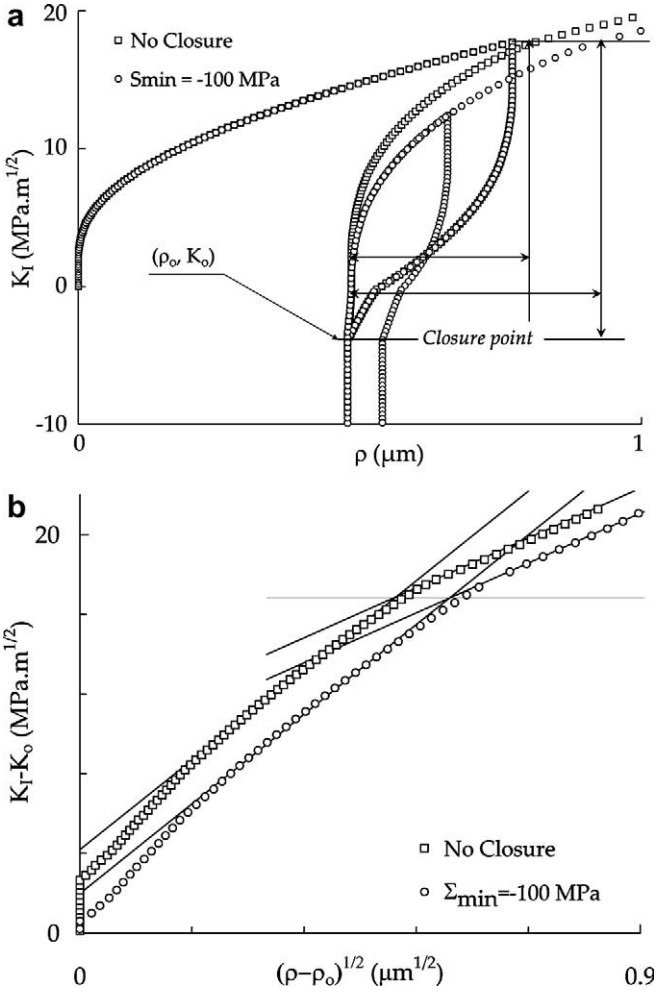

Fig. 9. (a) Computed evolutions of K_I and ρ, with or without a compression phase below the closure point. (b) idem, from the re-opening point in a $(K - K_0, (\rho - \rho_0)^{1/2})$.

An example of such computations is given in Fig. 9. Three main conclusions can be drawn from these computations. First of all, there is a very significant effect of the compression phase below the closure point on the evolution of ρ after the crack's re-opening (Fig. 9a). For the same variation of the stress intensity factor above the re-opening point the variation of ρ is at least 20% larger if a compression down to $\Sigma_{min} = -100$ MPa is applied. However, if the crack is unloaded, the closure point is not modified (Fig. 9a). This is the second important result: a compression phase below the closure point does not modify the position of this closure point. The third result is that the threshold at which the monotonic plastic zone extends itself is not modified (Fig. 9b). And finally, though it is not obvious in Fig. 9, it is also found that the size of the elastic domain of the cyclic plastic zone is not modified by a compression phase below the closure point. As a consequence, neither the position ϕ_X^m (closure point) and the size ϕ_{th}^m of the monotonic plastic zone, nor the size of the cyclic plastic zone ϕ_{th}^c vary during a compression phase. The only internal variable that is varying is the position ϕ_X^c of the cyclic plastic zone. It is also shown through these computations that the position of the elastic domain of the cyclic plastic zone is merely varying like K_{min}.

4.2. Comparison with experimental results

Therefore, in the model, the elastic domain for the cyclic plastic zone is allowed to be displaced below the closure point during the compression phase, this displacement simply follows the applied stress intensity factor K_{min}. Because of that displacement, the evolution law of the plastic flow intensity factor above the closure point is different. This simple modification of the model is sufficient to reproduce successfully the experimental results (Fig. 10).

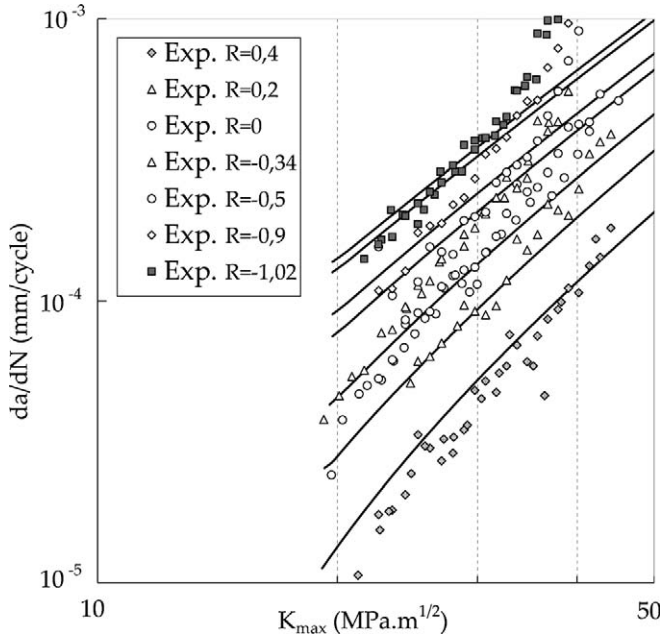

Fig. 10. Comparison between experimental results (symbols) and simulations (lines) for constant amplitude fatigue crack growth experiments at stress ratios R varying between 0.4 and -1.

The physical meaning of the displacement of the elastic domain of the cyclic plastic zone below the contact point is not obvious. It is possible to argue that "closure" corresponds to the first contact between the crack faces, which occurs at a rather large distance from the crack tip. But, in the near crack tip region, a "bump" remains behind the crack tip. When a compression phase is applied below the closure point, this bump is erased. This implies a modification of the state of internal stresses in the cyclic plastic zone. In our modelling, such a modification is modelled by a displacement of the elastic domain of the cyclic plastic zone.

5. Biaxial loading conditions

Now, the second feature of the industrial problem is that the crack is subjected to biaxial loading. Let consider the case of a through thickness crack in an infinite sheet subjected to a biaxial loading (S_x, S_y), the stress intensity factor and the T-stress are expressed as follows: $K_I = S_y\sqrt{\pi a}$ and $T = S_x - S_y$.

The idea is to show that it is possible to account for the effect of biaxial loading through the T-stress. For this purpose, finite element computations were performed so as to study the effect of the T-stress on the (ρ, K_I) curves.

5.1. Finite element analyses

For this analysis the material constitutive model that was employed was elastic, ideally plastic ($E = 200$ GPa, $v = 0.3$, $Re = 400$ MPa). Two finite element meshes were built with the same refinement at crack tip, but with two different crack dimensions $2a = 12$ mm and $2a = 24$ mm. The same method was employed in both cases so as to determine ρ from the displacement fields. The two cracks were loaded up to the same value of the maximum stress intensity factor K_I and then unloaded. In such a case the T-stress is lower at the tip of the smallest crack, since $T = -S_y = -K_I/\sqrt{\pi a}$. The results of this computation is plotted in Fig. 11a. It is obvious that the two cracks behave in a different manner. The plastic flow intensity factor ρ is larger for the smallest crack. If now the same values of K_I and of T are applied, by applying a suitable biaxial loading state, the same evolution of ρ is obtained for the two cracks (Fig. 11b). Two conclusions arise from these results. First of all, there is a significant effect of a biaxial stress loading condition on the evolution of the plastic flow intensity factor and secondly this effect can be characterized by the parameter (T/K_I) (see Fig. 12).

In the following, the biaxiality ratio is defined by the parameter (T/K_I).

Since an automated protocol was built up, so as to identify automatically the parameters of the model using finite element computations, it is easy to perform a set of

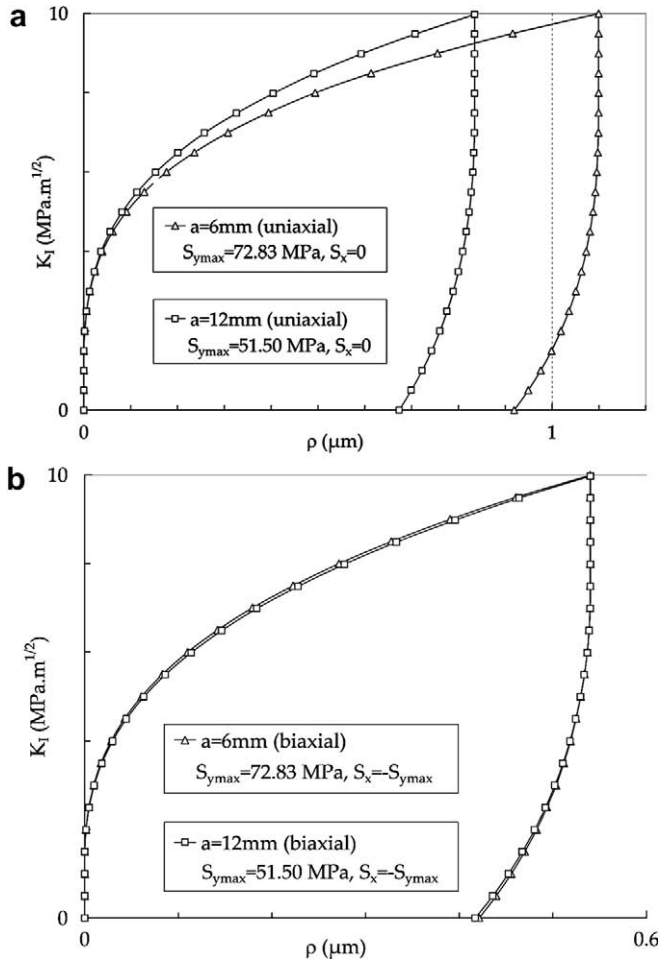

Fig. 11. Computed evolutions of K_I and ρ, for two cracks ($a = 6$ mm and $a = 12$ mm) (a) subjected to the same value of K_I, under a remote uniaxial loading condition and (b) to the same K_I and the same $T(T = 0)$.

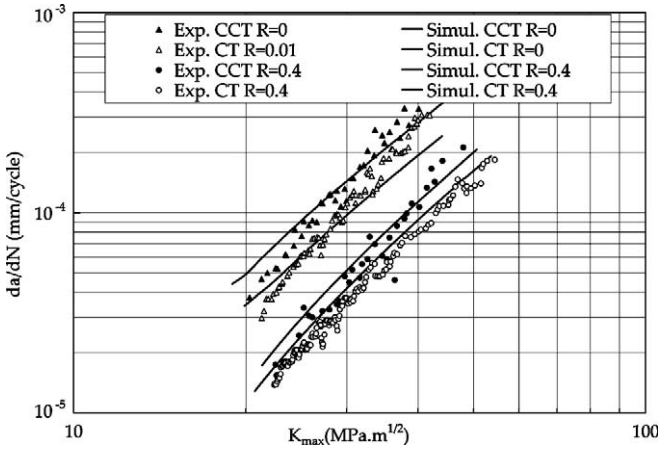

Fig. 12. fatigue crack growth rate at $R = 0$ and $R = 0.4$ in a CT and in a CC. Both specimens have the same thickness (5 mm) and were machined with the crack plane lying in the same direction of the train wheel. Comparison with the simulations.

identifications for a set of biaxiality ratios. This set of identifications was performed for the typical set of (T/K_I) ratios that are observed along the crack front of a semi-elliptical crack in the order of 1–10 mm, growing in a semi-infinite sheet subjected to a biaxial stress ($S_x = S_y/2$). It is worth to underline that the constitutive equations of the model have been chosen so as to fit the finite element results but also so as to ensure that a unique set of parameter is identified in each case. Therefore, it is possible to interpolate the set of identified parameters with respect to the ratio (T/K_I) using for instance polynomials. The results are provided in Appendix 2.

The expressions of the evolutions of the parameters of the model with respect to the biaxiality ratio (T/K) were implemented in the model so as to simulate the effect of a biaxial loading condition on fatigue crack growth.

5.2. Experimental results

So as to characterize the effect of the T-stress, complementary fatigue crack growth experiments have been performed on CT specimens. These specimens were machined from the train wheel. The same thickness (5 mm) was used for the CT and the CCT specimens (the expression of K_I and T for both specimens are given in Appendix 3). Attention was paid to machine them with their crack plane lying in the same plane as that of CCT specimens. CT and CCT specimen display a very different T/K_I ratio. While this ratio is negative in CCT specimen, it becomes positive in CT specimens (see Appendix 3).

In the experiment it is observed that the fatigue crack growth rate is nearly 1.7 higher in CCT specimen in comparison with the crack growth rate in CT specimens. This confirms the role of the T-stress on the fatigue crack growth rate. Besides, this difference is observed both at $R = 0.4$ and $R = 0$, but is larger at $R = 0.4$. The simulations are in reasonable agreement with the experimental results. Both the effect of the T-stress and the fact that this effect is larger at $R = 0.4$ than at $R = 0$ is reproduced by the model.

6. Conclusions

An incremental model for fatigue crack growth under complex loading conditions, which was proposed in previous publications, was identified, validated and modified so as to be applied to the problem of a semi-elliptical crack growing at the surface of a train's wheel.

For this purpose, push–pull experiments were conducted so as to identify the stress–strain behaviour of the medium carbon steel employed for the wheels. The material is found to be isotropic and its behaviour was modelled by three non-linear kinematics hardening and one non-linear isotropic hardening.

Then finite element analyses were conducted so as to compute the detail of the cyclic stress–strain behaviour in the crack tip region. A post-treatment routine was applied so as to identify the cyclic behaviour of the crack structure at the global scale from local FE computations. More

precisely, the evolutions of the plastic flow intensity factor were computed as a function of the applied stress intensity factors in various cases. Then, an empirical model was associated to these evolutions, for which the parameters were identified for the material of the wheel. The model was implemented and allows predicting the fatigue crack growth rate with the assumption that the fatigue crack growth rate is directly proportional to the plastic flow intensity factor rate. Fatigue crack growth experiments including overloads, and block loadings were compared to the predictions of the model and the results are satisfactory.

However, so as to apply this model to the industrial case of the train wheel, some developments had to be done. As a matter of fact, a train wheel was instrumented so as to measure strains in situ. It was found that, in the most critical area, the stress field across the wheels thickness can be considered as the sum of a biaxial bending loading case and of a biaxial tension-compression loading case. Therefore, the role of compressive stresses and of a biaxial stress state had to be considered.

The biaxial stress state was accounted for through the biaxiality parameter (T/K). The comparison between experimental fatigue crack growth rates within either CCT specimens or CT specimens, both at $R = 0$ and $R = 0.4$, showed that the T-stress has a significant effect on fatigue crack growth. The finite element method was employed so as to determine the evolutions of the parameters of the fatigue crack growth model as a function of the biaxiality ratio (T/K). These evolutions were implemented in the model and it was found that experiments and simulations are in good agreement.

The effect of compressive stresses was studied using the finite element method and fatigue crack growth experiments at various stress ratios, with R varying between -1 and 0.5. It was shown that neither the crack closure point, neither the size of the monotonic plastic zone, nor the size of the cyclic plastic zone are modified by a compressive overload below the closure point. However, the position of the elastic domain of the cyclic plastic zone is displaced. The model was modified so as to take into account this displacement, and a good agreement is obtained between the simulations and the experiments.

Appendix 1. Set of equations

We use the following relationships between the stress intensity factor and φ:

$$\phi = A^2K^2\text{signe}(K) \quad \text{with} \quad A = \sqrt{\frac{1-\nu^2}{2E}}$$

Extension of the monotonic plastic zone: $f_m = 0$ and $\frac{d\phi}{dt} > 0$

- Cracking law: $\frac{da}{dt} = \frac{\alpha}{2}\frac{d\rho}{dt}$
- Plastic criterion $(\phi_{xm} < \phi) : f_m = \sqrt{(\phi - \phi_{xm})^2} - \phi_m$
- Flow rule: $\frac{d\rho}{dt} = \lambda\frac{\partial f_m}{\partial \phi}$
- Consistence: $f_m = 0, \frac{df_m}{dt} = 0$
- Evolution equations:
  - $\frac{\partial \phi_{xm}}{\partial \rho} = a_{xm}\cdot\sqrt{\phi_{xm}}$
  - $\frac{\partial \phi_m}{\partial \rho} + \frac{\partial \phi_{xm}}{\partial \rho} = A^2a_m^2\frac{\sqrt{\phi_m+\phi_{xm}}}{\sqrt{\phi_m+\phi_{xm}}-Ab_m}$
  - $\frac{\partial \phi_m}{\partial a} = p_a\cdot\phi_m$
  - $\frac{\partial \phi_{xm}}{\partial a} = k_a\cdot\phi_{xm} + k_b.\phi_m \quad \text{with} \quad A^2 = \frac{(1-\nu^2)}{2E}$
- Material parameters (a_m, b_m, a_{xm}, p_a, k_a, k_b)
- Initial values: $\phi_{m0} = A^2b_m^2, \phi_{x0} = 0$

Extension of the cyclic plastic zone: $f_c = 0$

- Cracking law: $\frac{da}{dt} = \frac{\alpha}{2}\left\langle\frac{d\rho}{dt}\right\rangle$
- Plastic criterion: $f_c = \sqrt{(\phi - \phi_{xc})^2} - \phi_c$
- Flow rule: $\frac{d\rho}{dt} = \lambda\frac{\partial f_c}{\partial \phi}$
- Consistence: $f_c = 0, \frac{df_c}{dt} = 0$
- Evolution equations:
  - $\frac{\partial \phi_c}{\partial \rho} = \frac{\partial \phi_c}{\partial a} = \frac{\partial \phi_{xc}}{\partial a} = 0$
  - $\frac{\partial \phi_{xc}}{\partial \rho} = A^2\frac{a_c^2\sqrt{\phi_{xc}+\delta\cdot\phi_c}}{\delta\left(\sqrt{\phi_{xc}+\delta\cdot\phi_c}-\frac{\phi_c}{Ab_c}\right)-\frac{Ab_c}{2}}$ with $\delta = \text{sign}\frac{d\rho}{dt}$
  - $\frac{\partial \phi_m}{\partial a} = p_a\cdot\phi_m$
  - $\frac{\partial \phi_{xm}}{\partial a} = k_a\cdot\phi_{xm} + k_b\cdot\phi_m$ with $A^2 = \frac{(1-\nu^2)}{2E}$
- Material parameters (a_c, b_c)
- Evolutions of ϕ_c and ϕ_{xc} when the monotonic plastic zone is activated:

$$\phi = \phi_c + \phi_{xc} \quad \text{and} \quad \phi_c = \frac{A^2b_c}{2}\left(2\frac{\sqrt{\phi}}{A} - b_c\right)$$

Set of material parameters for $T = 0$:

$a_m = 17.3\ \text{MPa}\sqrt{\text{m}}/\mu\text{m}$

$b_m = 4.6\ \text{MPa}\sqrt{\text{m}}$

$a_{cf} = 38.2\ \text{MPa}\sqrt{\text{m}}/\mu\text{m}$

$b_{cf} = 5.8\ \text{MPa}\sqrt{\text{m}}$

$a_{xm} = -1.5\ \text{MPa}\sqrt{\text{m}}/\mu\text{m}$

$p_a = -0.00093\ \text{MPa}\sqrt{\text{m}}/\mu\text{m}$

$k_a = -0.019\ \text{MPa}\sqrt{\text{m}}/\mu\text{m}$

$k_b = 0.0025\ \text{MPa}\sqrt{\text{m}}/\mu\text{m}$

Appendix 2.

Evolution of the material parameters for various values of the biaxiality ratio (T/K), and the fitted polynomials implemented in the model.

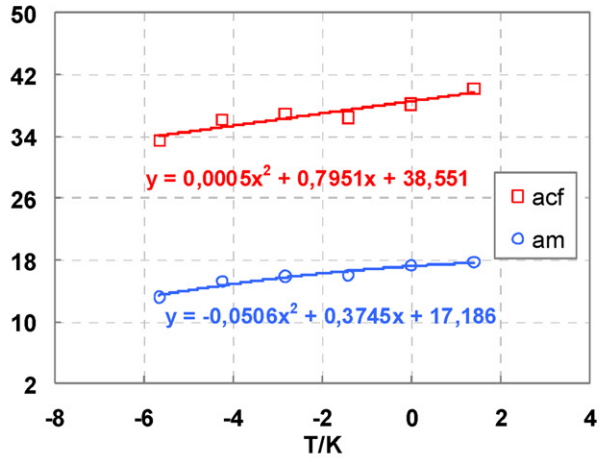
y = 0,0005x² + 0,7951x + 38,551
y = -0,0506x² + 0,3745x + 17,186
acf
am
T/K

(a)

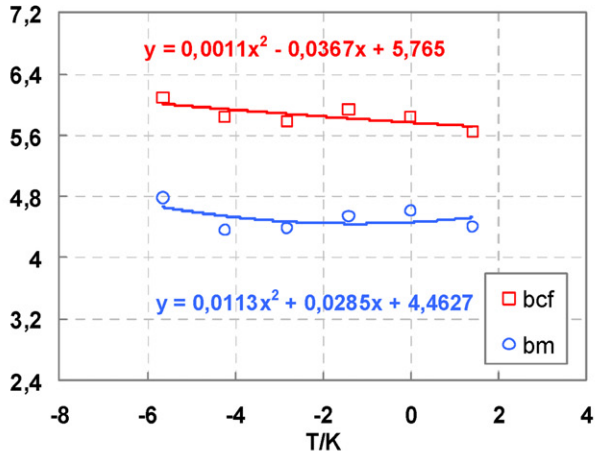
y = 0,0011x² - 0,0367x + 5,765
y = 0,0113x² + 0,0285x + 4,4627
bcf
bm
T/K

(b)

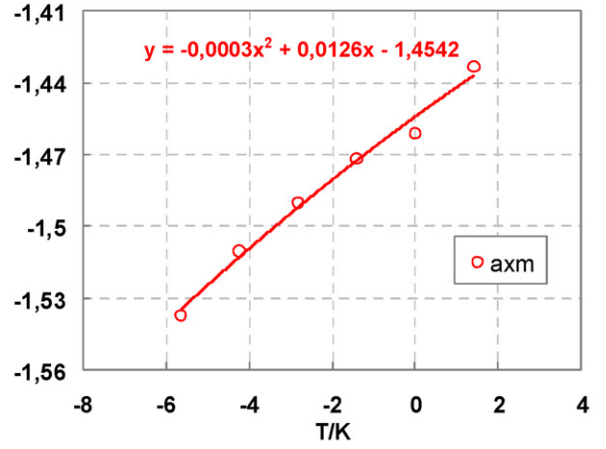
y = -0,0003x² + 0,0126x - 1,4542
axm
T/K

(c)

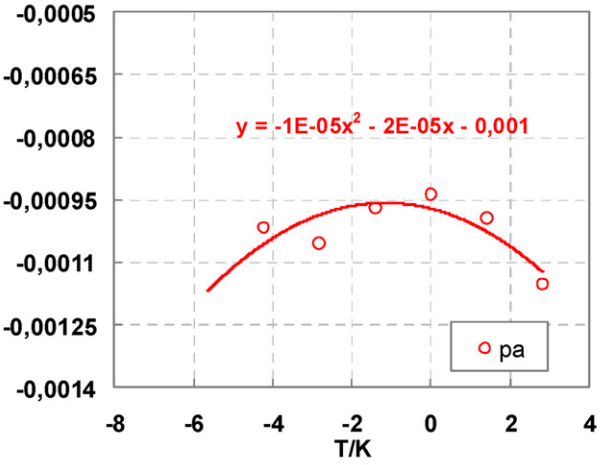
y = -1E-05x² - 2E-05x - 0,001
pa
T/K

(d)

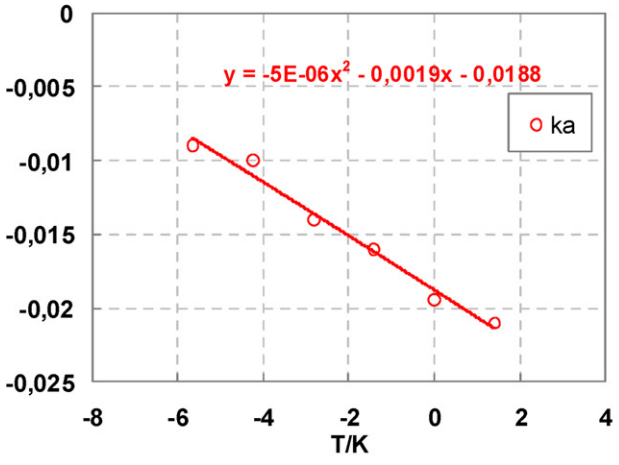
y = -5E-06x² - 0,0019x - 0,0188
ka
T/K

(e)

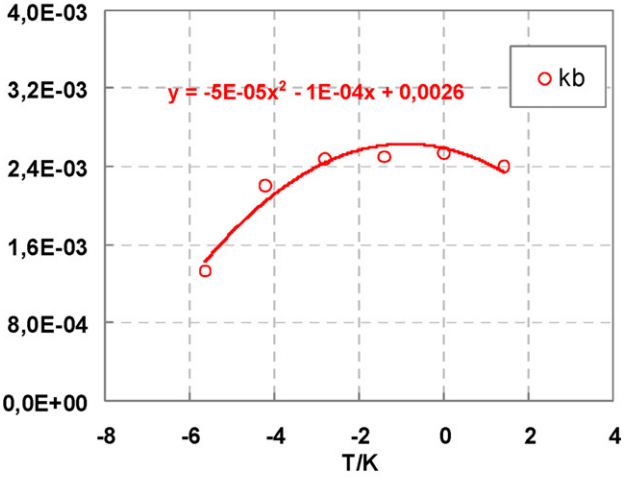
y = -5E-05x² - 1E-04x + 0,0026
kb
T/K

(f)

Appendix 3.

CCT specimen

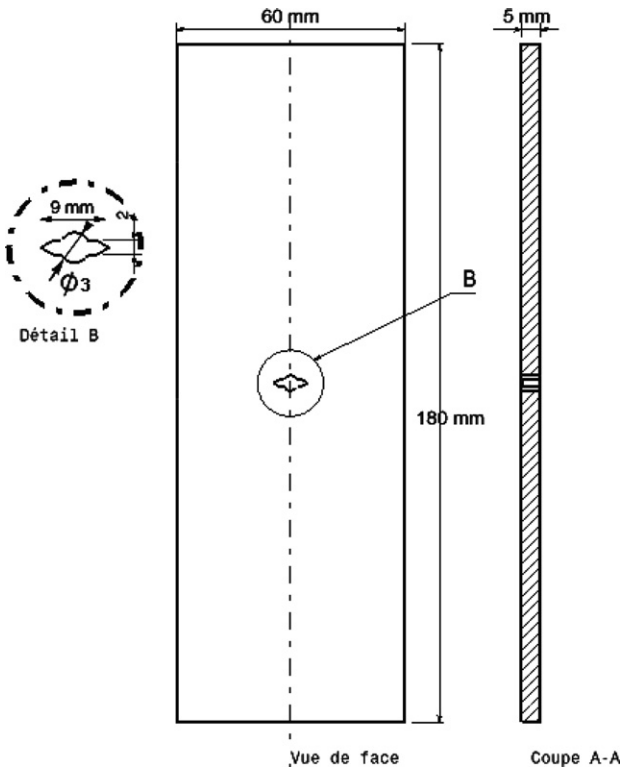

Expression of K [18]:

$$K = \frac{FY}{BW^{\frac{1}{2}}} \quad \text{if} \quad F > 0$$
$$K = 0 \quad \text{if} \quad F \leqslant 0$$

With:
B: specimen thickness
W: specimen width
F: applied force N
Y: shape factor given by:

$$Y = \left(\frac{\theta}{\cos\theta}\right)^{\frac{1}{2}}(0.707 - 0.007\theta^2 + 0.007\theta^4) \quad \text{and} \quad \theta = \frac{\pi a}{2W}$$

Expression of T [19]:

$$T = S_y\left(-0.997 + 0.283\frac{a}{w} - 3.268\left(\frac{a}{w}\right)^2 + 6.622\left(\frac{a}{w}\right)^3 - 5.995\left(\frac{a}{w}\right)^4\right)$$

With:
Sy: Applied stress MPa.
CT specimen

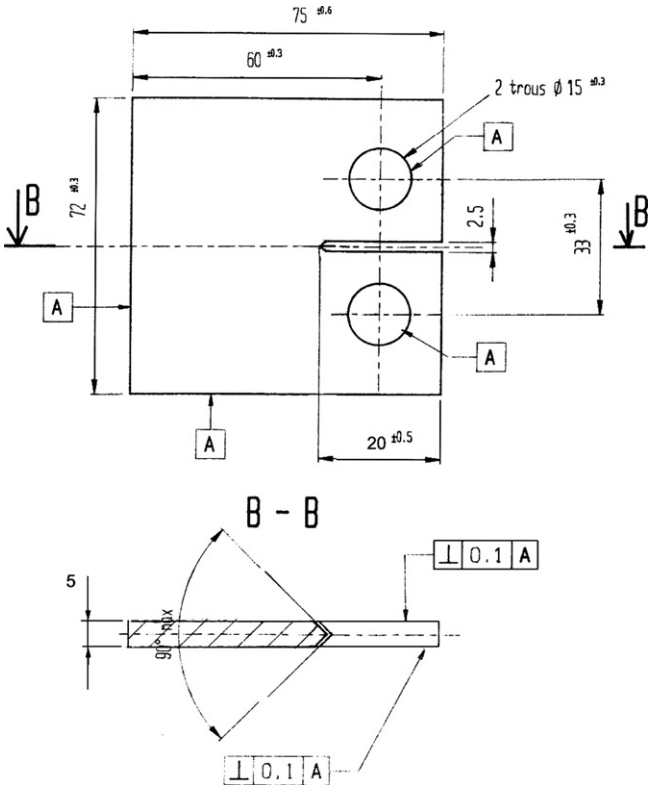

Expression of K [18]:

$$K = \frac{FY}{BW^{\frac{1}{2}}} \quad \text{with} \quad F > 0$$

With:
B: specimen thickness
W: specimen width
F: applied force N
Y: shape factor given by:

$$Y = (2+\theta)\frac{(0.886 + 4.64\theta - 13.32\theta^2 + 14.72\theta^3 - 5.6\theta^4)}{(1-\theta)^{1.5}}$$

and $\theta = \frac{a}{W}$

Expression of T [19]:

$$T = S_y\left(-1.996 + 10.169\frac{a}{w} + 10.546\left(\frac{a}{w}\right)^2\right)$$

With:
Sy: Applied stress MPa given by $S_y = \frac{F}{W \cdot B}$.

References

[1] Forman RG, Kearney VE, Engle RM. Numerical analysis of crack propagation in cyclic loaded structures. J Basic Eng 1967;89:459–64.
[2] Pelloux RMN. Mechanisms of formation of ductile fatigue striations. Trans ASM 1969;62:281–5.
[3] Elber W. The significance of fatigue crack closure. ASTM STP 1971;468:230–42.

[4] Wheeler O. Spectrum loading and crack growth. J Basic Eng 1972;94:181–6.
[5] Schijve J. The significance of fractography for investigations of fatigue crack growth under variable amplitude fatigue. Fatigue Fract Eng Mater Struct 1999;22:87–99.
[6] Skorupa M. Load interaction effects during fatigue crack growth under variable amplitude loading – a literature review Part II: qualitative interpretation. Fatigue Fract Eng Mater Struct 1999;22(10):905–26.
[7] Pommier S, Risbet M. Time-derivative equations for fatigue crack growth in metals. Int J Fract 2005;131(1):79–106.
[8] Pommier S. Cyclic plasticity and variable amplitude fatigue. Int J Fatigue 2003;25(9-11):983–97.
[9] Pommier S, De Freitas M. Effect on fatigue crack growth of interactions between overloads. Fatigue Fract Eng Mater Struct 2002;25:709.
[10] Dundurs J. Elastic interaction of dislocations with inhomogeneities. In: Mura T, editor. Mathematical theory of dislocations. New York: ASME; 1969. p. 0–115.
[11] Lakshmanan V, Li JCM. Edge dislocations emitted along inclined planes from a mode I crack. Mater Sci Eng A 1988;104(10):95–104.
[12] Pommier S, Hamam R. Incremental model for fatigue crack growth base on a projection hypothesis for mode I elastic–plastic displacements fields. FFEMS, in press.
[13] Pommier S. Cyclic plasticity of a cracked structure submitted to mixed mode loading. In: Khan AS, Kazmi R, editors. Proceedings of PLASTICITY '06, Halifax, Canada, 17–22 Juillet, 2006.
[14] Pommier, S. Cyclic plasticity of a cracked structure submitted to mixed mode loading. Plasticity '06 – 12th International Symposium on Plasticity and its Current Applications. Halifax, Nova Scotia, Canada, 17–22 July; 2006.
[15] Newman JC, Raju IS. An empirical stress-intensity factor equation for the surface crack. Eng Fract Mech 1981;15: 185–92.
[16] Wang X. Elastic *T*-stress solutions for semi-elliptical surface cracks in finite thickness plates. Eng Fract Mech 2003;70:731–56.
[17] McClintock FA. Discussion to C. Laird's paper "The influence of metallurgical microstructure on the mechanisms of fatigue crack propagation". Fatigue Crack Propagation, ASTM STP 415. 1967. p. 170–4.
[18] Normalisation française, June 1991, Pratique des essais de vitesse de propagation de fissure en fatigue, A03-404.
[19] Sherry AH, France CC, Goldthorpe MR. Compendium of *T*-stress solution for two and three dimensional cracked geometries. Fatigue Fract Eng Mater Struct 1995;18:141–55.